Journal of ELECTRONIC MATERIALS, Vol. 44, No. 6, 2015
DOI: 10.1007/s11664-014-3411-z
© 2014 The Minerals, Metals & Materials Society

Effect of Sintering Temperature on Thermoelectric Properties of PbTe/Ag Composites Fabricated by Chemical Plating and Spark Plasma Sintering

F.R. SIE,[1,2] C.S. HWANG,[1,4] Y.H. TANG,[1] C.H. KUO,[1,3] Y.W. CHOU,[2] C.H. YEH,[2] H.Y. HO,[2] Y.L. LIN,[2] and C.H. LAN[2]

1.—Department of Materials Science and Engineering, National Cheng Kung University, Tainan City 701, Taiwan. 2.—Green Energy & Environment Laboratories, Industrial Technology Research Institute, Hsinchu City 310, Taiwan. 3.—China Steel Corporation, Kaohsiung City 812, Taiwan. 4.—e-mail: cshwang@mail.ncku.edu.tw

PbTe/Ag composite powders were synthesized by a chemical plating method and then compacted by spark plasma sintering (SPS) at 573 K to 673 K and 50 MPa. The effects of the sintering temperature on the thermoelectric properties of PbTe and the PbTe/Ag composites were investigated. The thermoelectric properties of PbTe and PbTe/Ag bulk samples were measured in the temperature range from 300 K to 700 K. PbTe/Ag bulk samples changed electrical transport behavior from *p*-type to *n*-type at room temperature. The SPS temperature not only changed the lattice parameter but also affected the conduction behavior of PbTe/Ag composites. The variation in the carrier concentration was determined by the role of the Ag dopant for different SPS temperatures. Moreover, the conduction of the PbTe/Ag samples changed from metallic to semiconducting in the measured temperature range from 300 K to 700 K as the sintering temperature increased. For the PbTe/Ag bulk materials subjected to SPS at 573 K and 673 K, the values of the power factor were 0.38 mW/m K^2 and 1.31 mW/m K^2 at 700 K, respectively.

Key words: PbTe, PbTe/Ag composites, spark plasma sintering, sintering temperature, power factor

INTRODUCTION

PbTe and its alloys have optimal thermoelectric properties in the temperature range from 500 K to 800 K.[1] In recent studies, PbTe alloys have been decorated with nanostructures to improve their thermoelectric performance, leading to decreased thermal conductivity; For example, Hsu et al.[2] reported that the thermoelectric properties of *n*-type $AgPb_mSbTe_{m+2}$ (LAST-*m*, $m = 10$ and $m = 18$) alloys were enhanced to $ZT = 2.2$ at 800 K with nanosized Ag-Sb-rich inclusions. Pei et al.[3] observed that nanoscale CdTe precipitates were dispersed in the PbTe-CdTe bulk, which caused the lattice thermal conductivity decrease, and that the bulk had a ZT of 1.7 in the temperature range of 700 K to 800 K. In addition, electronic energy filtering due to fine grain size (i.e., nanograins) increased the Seebeck coefficient and decreased the lattice thermal conductivity, thus improving the thermoelectric properties of the PbTe alloys.[4–6] Furthermore, it is reported that heterostructures in thermoelectric materials resulting from hydrothermal treatment could reduce the lattice thermal conductivity without compromising the Seebeck coefficient or electrical conductivity.[7–9]

In this study, a novel process involving electroless silver plating and SPS was used to fabricate PbTe/Ag bulk composites with heterogeneous structures. The effects of the sintering temperature on the

(Received July 16, 2014; accepted September 5, 2014; published online September 23, 2014)

thermoelectric performance of the PbTe and PbTe/Ag bulk materials are investigated.

EXPERIMENTAL PROCEDURES

Commercial PbTe ingots (99.98%; Alfa Aesar) were crushed and sieved to obtain sub-75-μm-diameter powders. PbTe/Ag composite powders were synthesized by an electroless silver plating method. The compositions of the solutions used for electroless silver plating, with glucose and tartaric acid as the reducing agent, are presented in Table I. First, a $SnCl_2$ and HCl mixed solution was used as the sensitizer, in which PbTe powders were immersed for 5 min. Second, the sensitized PbTe powders were put into the electroless plating bath for 15 min with the reducing agent. The hybrid powders were then washed and centrifuged with deionized water, and dried at 373 K in a vacuum oven. Finally, PbTe and PbTe/Ag compacts were sintered at 573 K, 623 K, and 673 K, respectively, by spark plasma sintering (SPS, Dr. Sinter, SPS-systex) at uniaxial pressure of 50 MPa under Ar atmosphere.

Phase identification for the bulk samples was confirmed by x-ray diffraction (XRD, D5000, Siemens) at room temperature using Cu K_α radiation (λ = 0.15406 nm). The microstructures of the samples were observed using field-emission scanning electron microscopy (FE-SEM; 7000F, JEOL). The compositions of the PbTe and PbTe/Ag hybrid powders were analyzed by inductively coupled plasma mass spectrometry (ICP-MS), and the results are presented in Table II. The bulk samples were cut into rectangular bars (3 mm × 3 mm × 15 mm) for measurement of the electrical conductivity and Seebeck coefficient under a low inert-gas atmosphere at temperature ranging from 300 K to 700 K using commercial equipment (ZEM-3; Ulvac Riko, Inc.). The carrier concentration and mobility were measured using four-probe Hall-effect measurements at room temperature.

RESULTS AND DISCUSSION

Figure 1 shows the XRD patterns of PbTe and PbTe/Ag bulk samples subjected to SPS at various temperatures. Only PbTe and Ag crystalline phases existed in all the PbTe/Ag samples, and the intensity of Ag increased along with the SPS temperature, as shown in Fig. 1a and b. The lattice parameters for PbTe and PbTe/Ag subjected to different temperatures are presented in Table III. The lattice parameter of PbTe was 6.4491 Å, 6.4409 Å, and 6.4406 Å, while that of PbTe/Ag was 6.4611 Å, 6.4585 Å, and 6.4521 Å at the different SPS temperatures. With increasing sintering temperature, both lattice parameters decreased. In addition, the parameter was larger for the PbTe/Ag samples than for the PbTe samples. Schenk et al.[10] demonstrated

Table I. Components and concentrations for electroless silver plating

Component	Concentration (M)
$SnCl_2$	0.06
HCl	1
$AgNO_3$	0.3
NaOH	0.9
NH_4OH	2
Glucose	0.25
Tartaric acid	0.03

Table II. Composition ratios of PbTe and PbTe/Ag powders

Sample	Pb (at.%)	Te (at.%)	Ag (at.%)
PbTe	48.95	51.05	0
PbTe/Ag	42.32	44.12	13.55

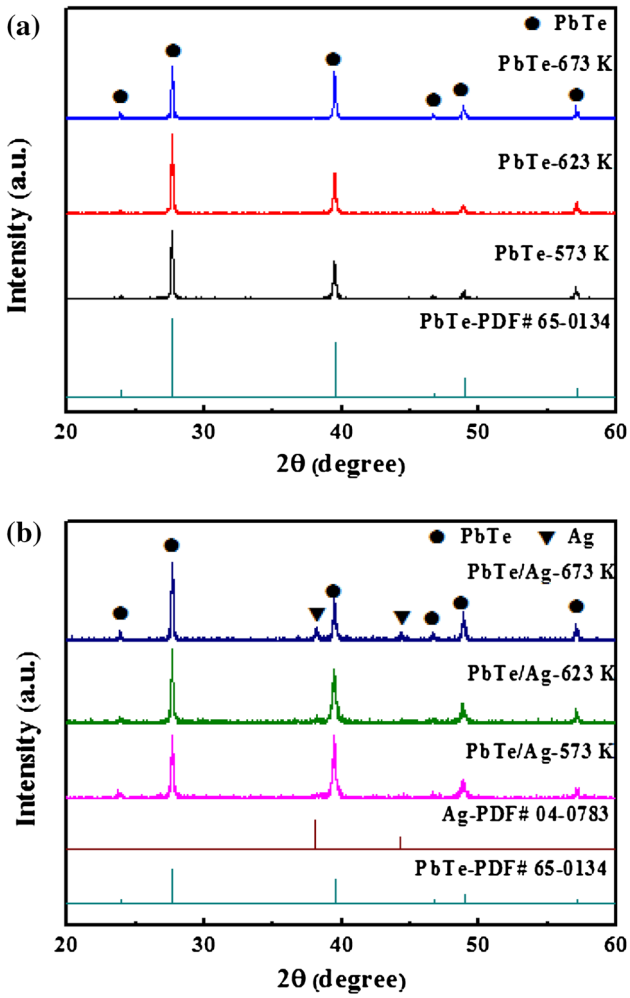

Fig. 1. XRD patterns of (a) PbTe and (b) PbTe/Ag bulk samples prepared by electroless silver plating and subjected to SPS at various temperatures.

that volatilization of Pb could produce excessive Pb vacancies in PbTe (Te-rich) with increasing sintering temperature. Pb vacancies caused the lattice parameter of PbTe to decrease, consistent with the results in Table III. The ionic radii of Ag^{+}, Pb^{2+}, and Te^{2-} are 1.13 Å, 1.32 Å, and 2.11 Å, respectively. Generally, the lattice parameter decreases as Ag^{+} ions substitute at Pb^{2+} sites because the metallic ionic radius of Ag (1.13 Å) is smaller than that of Pb (1.32 Å). However, all the PbTe/Ag samples had larger lattice parameters in this study. The results show that Ag^{+} lies at interstitial sites in PbTe. Strauss et al.[11] reported that the role of Ag is not only as an acceptor (Ag^{+} at Pb^{2+} sites of PbTe) but also as a donor (Ag^{+} at interstitial sites of PbTe) in Te-saturated and Pb-saturated single-crystal samples of PbTe produce by the Bridgman method. On the other hand, when SPS is carried out at high temperature, excessive Pb vacancies could be formed in PbTe, and Ag^{+} ions could then enter these vacancies, causing the lattice parameter of the PbTe/Ag samples to decrease. Therefore, Ag^{+} can occupy interstitial sites and substitutional sites at Pb vacancies in the PbTe at the same time.

Figure 2 displays SEM images of PbTe powder, PbTe/Ag hybrid powder, and corresponding bulk samples after sintering at 573 K to 673 K. The PbTe particles have smooth surfaces, on which Ag particles with size in the range from 50 nm to 200 nm agglomerated (Fig. 2a and b). The backscattered electron image of the polished surfaces of the PbTe/Ag bulk sintered at 673 K shows that Ag agglomerated (dark) in the PbTe matrix (bright) (Fig. 2c). The fracture surfaces of the PbTe/Ag samples show a dense morphology for higher sintering temperature (Fig. 2e and f). The relative density of the PbTe/Ag samples increased from 91.5% to 98.5% as the sintering temperature was increased from 573 K to 673 K, as shown in Table III, consistent with the SEM results.

The carrier concentration and mobility values of the PbTe and PbTe/Ag samples obtained using various SPS temperatures are listed in Table III. The carrier concentration of all PbTe samples showed positive values, thus holes were the main contributors to electric charge transport. The carrier concentration increased from 9.81×10^{15} cm^{-3} to 2.60×10^{18} cm^{-3} as the sintering temperature was increased from 573 K to 673 K. In contrast, the carrier concentration of all the PbTe/Ag samples had negative values, meaning that electrons were the main contributors to electric charge transport. Moreover, the carrier concentration of the PbTe/Ag samples decreased from 1.14×10^{20} cm^{-3} to 1.03×10^{20} cm^{-3} with increasing sintering temperature. In addition, as the sintering temperature was increased, Pb evaporated and thus Pb vacancies were produced. The increase in the concentration of Pb vacancies at higher sintering temperature led to an increase in the carrier concentration of holes and a decrease in the lattice parameter of PbTe. When Ag clusters were embedded in the PbTe matrix, the conduction behavior changed from *p*-type (holes) to *n*-type (electrons). Ag clusters contributed excess electrons to transform the carrier type, which explains why the conduction characteristic of the PbTe/Ag samples changed. According to the results for the lattice parameter, Ag^{+} could play two roles in PbTe as the SPS temperature is increased. In the sintering process, Ag^{+} ions not only entered interstitial sites of the PbTe lattice as donors, but also replaced Pb^{2+} sites in the PbTe as acceptors. The two opposite carrier types caused carrier recombination and decreased the carrier concentration at high SPS temperature. Despite having the opposite carrier type to the PbTe/Ag samples, electrons remain the main electric charge transport carriers.

Figure 3 shows the temperature dependence of the Seebeck coefficient for all the sintered samples, measured from 300 K to 700 K. The Seebeck coefficient of the PbTe bulk samples decreased from 358 μV/K to 238 μV/K at room temperature as the sintering temperature was increased from 573 K to 673 K. In contrast, all the Seebeck coefficient values of the PbTe/Ag samples were negative in the measured temperature range from 300 K to 700 K. The Seebeck coefficient of the PbTe/Ag samples increased slightly from 16 μV/K to 86 μV/K at room temperature with increasing SPS temperature. As seen in Fig. 3, the Seebeck coefficient of the PbTe and PbTe/Ag samples showed a converse conduction behavior at room temperature. The PbTe and PbTe/Ag samples were *p*- and *n*-type conductors at room

Table III. Carrier concentration, mobility, lattice parameter, and relative density of PbTe and PbTe/Ag bulk samples for different sintering temperatures

Sample	Type (*p*/*n*)	Carrier Concentration (cm^{-3})	Mobility (cm^2/Vs)	Lattice Parameter (Å)	Relative Density (%)
PbTe-300°C	*p*	9.81×10^{15}	1.52×10^{2}	6.4491	97.1
PbTe-350°C	*p*	2.78×10^{17}	6.20×10^{2}	6.4409	98.6
PbTe-400°C	*p*	2.60×10^{18}	8.37×10^{2}	6.4406	98.6
PbTe/Ag-300°C	*n*	1.14×10^{20}	1.21×10^{2}	6.4611	91.5
PbTe/Ag-350°C	*n*	1.82×10^{19}	1.59×10^{2}	6.4585	94.9
PbTe/Ag-400°C	*n*	1.03×10^{19}	1.56×10^{2}	6.4521	98.5

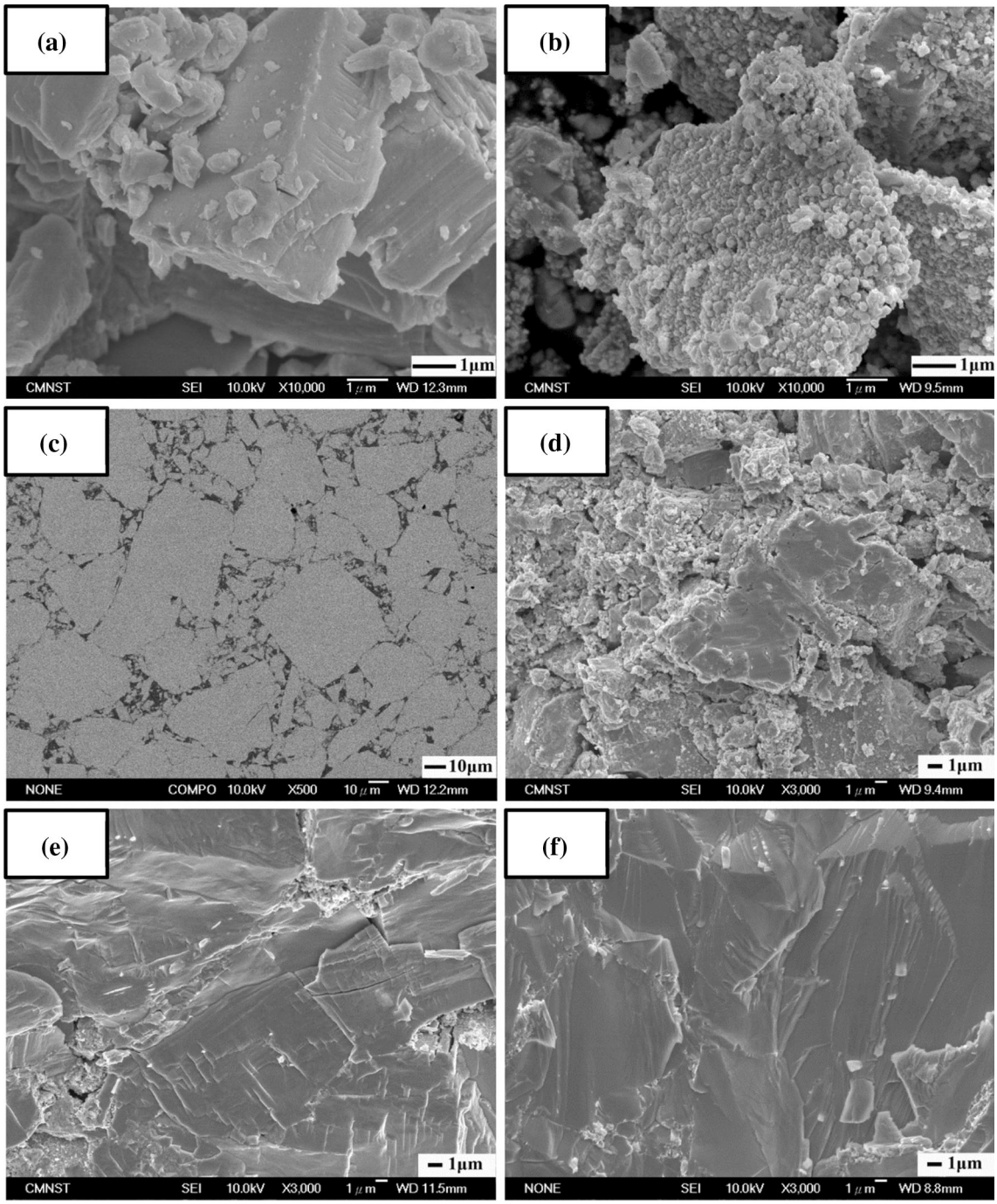

Fig. 2. SEM images of (a) PbTe powder, (b) PbTe/Ag hybrid powder, (c) polished surfaces of PbTe/Ag bulk sample fabricated by SPS at 673 K, and fracture surfaces of PbTe/Ag bulk samples fabricated by SPS at (d) 573 K, (e) 623 K, and (f) 673 K.

temperature, respectively, as confirmed by the Hall-effect measurements. Because extra Pb vacancies were produced, this increased the carrier concentration of holes and decreased the Seebeck coefficient. Additionally, PbTe has a bipolar characteristic, meaning that the conduction behavior can be transformed from *p*- to *n*-type with increasing measurement temperature. However, the agglomeration of Ag produced extra electrons in the PbTe/Ag samples during SPS, so the conduction behavior changed from *p*- to *n*-type. At higher SPS temperature, Ag^{+} ions could rapidly diffuse into interstitial sites of PbTe and simultaneously substitute Pb^{2+} ions in the PbTe. When Ag^{+} ions occupied Pb vacancies and contributed excess holes in PbTe/Ag samples at higher sintering temperature, the carrier concentration would decrease, causing the Seebeck coefficient to increase.

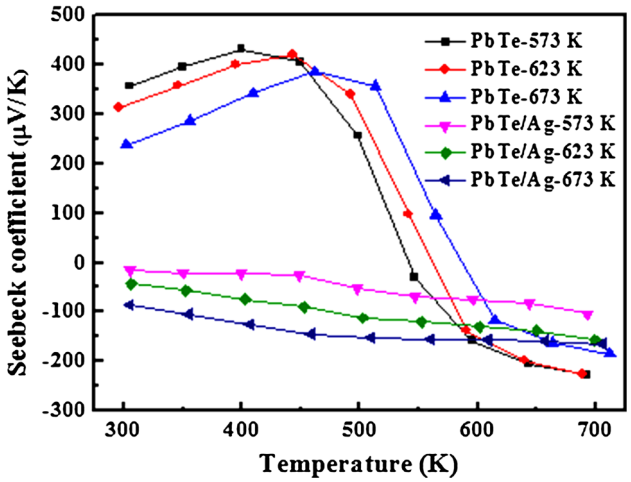

Fig. 3. Temperature dependence of Seebeck coefficient for PbTe and PbTe/Ag samples prepared by electroless silver plating with sintering at various temperatures.

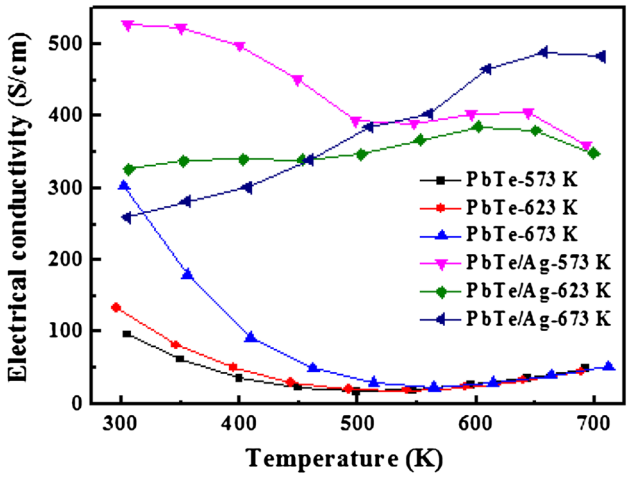

Fig. 4. Temperature dependence of electrical conductivity for PbTe and PbTe/Ag samples prepared by electroless silver plating with sintering at various temperatures.

Figure 4 shows the temperature dependence of the electrical conductivity for all the sintered samples. The electrical conductivity of the PbTe specimens increased from 96 S/cm to 303 S/cm at room temperature as the sintering temperature was increased from 573 K to 673 K. Over the whole measured temperature range from 300 K to 700 K, the electrical conductivity exhibited bipolar conduction behavior. Generally, a higher SPS temperature led to evaporation of Pb from the PbTe and created Pb vacancies, thus increasing the carrier concentration of holes. Moreover, a higher sintering temperature also could result in an increase in grain size and thus the relative density of the PbTe samples, improving the mobility of PbTe. Therefore, the electrical conductivity was increased at high sintering temperature, due to an increase in the carrier concentration of holes and mobility at the same time. Additionally, the electrical conductivity of the PbTe still appears to exhibit bipolar conduction, which is attributed to excitation of intrinsic electronic carriers at high temperature.

In contrast, the electrical conductivity of the PbTe/Ag specimens decreased from 527 S/cm to 259 S/cm at room temperature as the sintering temperature was increased from 573 K to 673 K. Based on these results, for different SPS temperatures, the electrical conductivity of the PbTe/Ag samples was greater than that of the PbTe samples in the measured temperature range from 300 K to 700 K. All the PbTe/Ag samples had higher carrier concentration of electrons because the Ag clusters provide a larger amount of electrons to converse the electric charge transport of PbTe. According to the Hall-effect measurements and Seebeck coefficient results, there are two defect types with Ag^+ ions located in the PbTe system at different sintering temperatures. During the sintering process, Ag^+ ions at interstitial sites of the PbTe lattice act as donors through SPS. When the sintering temperature is increased, PbTe creates more Pb vacancies, into which Ag^+ ions enter, which decreases the carrier concentration and electrical conductivity. Moreover, the conduction of PbTe/Ag samples changed from metallic to semiconducting in the measured temperature range from 300 K to 700 K as the sintering temperature was increased, as shown in Fig. 4. At lower SPS temperature, the Ag clusters contributed a larger number of electrons and shifted the Fermi level into the conduction band of PbTe as a degenerate semiconductor (metallic). This degenerate semiconductor nature will cause the electrical conductivity to decrease with increasing measurement temperature. However, for SPS temperature of 673 K, the results show a semiconductor characteristic over the whole measured temperature range. A phenomenon of conversion between metallic and semiconducting behavior can be observed at different SPS temperatures. When the sintering temperature was increased from 573 K to 673 K, more Ag^+ ions would enter into substitutional and interstitial sites of PbTe at the same time, and the Fermi level shifted toward the valence band. Therefore, the decrease in the carrier concentration was due to the interaction of these defects, which led the conduction behavior to change from degenerate semiconducting (metallic) to semiconducting.

Figure 5 shows the temperature dependence of the power factor ($S^2\sigma$) for all the bulk samples. The power factor of the PbTe/Ag specimens was larger than those of all the PbTe specimens at high measurement temperature. Moreover, the power factor of all the PbTe/Ag samples increased with higher measurement temperature. A maximum value of 1.31 mW/m K^2 was obtained at 700 K for the PbTe/Ag bulk sample sintered at 673 K, owing to its large electrical conductivity of 483 S/cm and relatively

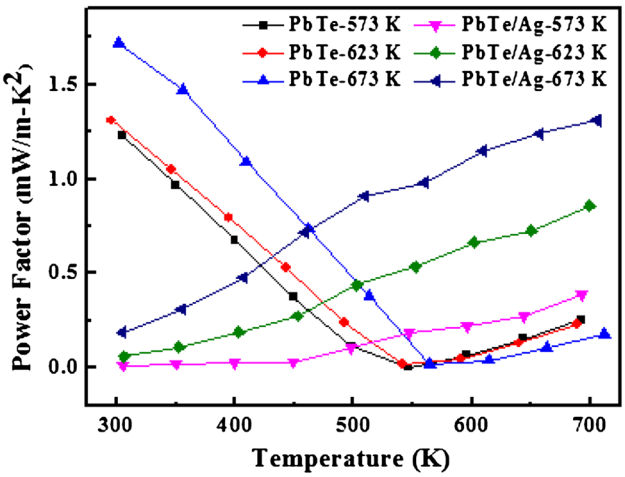

Fig. 5. Temperature dependence of power factor for PbTe and PbTe/Ag samples prepared by electroless silver plating with sintering at various temperatures.

high Seebeck coefficient of 165 μV/K at high measurement temperature. Even though the power factor value in this work is not high enough, these experimental results demonstrate that adjusting the chemical treatment and sintering temperature can still optimize the thermoelectric transport properties of PbTe bulk materials.

CONCLUSIONS

PbTe/Ag thermoelectric composites were successfully synthesized by a chemical plating method and SPS. Different sintering temperatures led to different thermoelectric properties of the PbTe and PbTe/Ag bulk samples. The relation between Pb vacancies and Ag^+ ions has an impact on the conduction behavior with increasing sintering temperature, enhancing the electrical conductivity and Seebeck coefficient at high measurement temperature. Further thermal conductivity measurements are required to evaluate the processing technique in this work as a route to optimize the thermoelectric performance of PbTe/Ag bulk materials.

ACKNOWLEDGEMENTS

The authors would like to thank the Bureau of Energy, Ministry of Economic Affairs of Republic of China, for financially supporting this work.

REFERENCES

1. V. Fano, *CRC Handbook of Thermoelectrics*, ed. D.M. Rowe (Boca Raton, FL: CRC, 1995), p. 257.
2. K.F. Hsu, S. Loo, F. Guo, W. Chen, J.S. Dyck, C. Uher, T. Hogan, E.K. Polychroniadis, and M.G. Kanatzidis, *Science* 303, 818 (2004).
3. Y. Pei, A.D. LaLonde, N.A. Heinz, and G.J. Snyder, *Adv. Energy Mater.* 2, 670 (2012).
4. J.P. Heremans, C.M. Thrush, and D.T. Morelli, *Phys. Rev. B* 70, 115334 (2004).
5. J. Martin, L. Wang, L.D. Chen, and G.S. Nolas, *Phys. Rev. B* 79, 115311 (2009).
6. C.H. Kuo, H.S. Chien, C.H. Hwang, Y.W. Chou, M.S. Jeng, and Masahiro Yoshimura, *Mater. Trans.* 52, 795 (2011).
7. R. Jin, G. Chen, J. Pei, and C. Yan, *New J. Chem.* 36, 2574 (2012).
8. X. Ji, B. Zhang, Z. Su, T. Holgate, J. He, and T.M. Tritt, *Phys. Status Solidi A* 206, 221 (2009).
9. X. Ji, J. He, Z. Su, N. Gothard, and T.M. Tritt, *J. Appl. Phys.* 104, 034907 (2008).
10. M. Schenk, H. Berger, A. Klimakow, M. Müilberg, and M. Wienecke, *Cryst. Res. Technol.* 23, 77 (1988).
11. A.J. Strauss, *J. Electron. Mater.* 2, 553 (1973).